

# Safe Pati-Salam

E. Molinaro<sup>1</sup>, F. Sannino<sup>2,3</sup>, Z.W. Wang<sup>2,4</sup>

<sup>1</sup>*Department of Physics and Astronomy, University of Aarhus,  
Ny Munkegade 120, DK-8000 Aarhus C, Denmark*

<sup>2</sup>*CP<sup>3</sup>-Origins, University of Southern Denmark,  
Campusvej 55, DK-5230 Odense M, Denmark*

<sup>3</sup>*Danish IAS, University of Southern Denmark, Denmark*

<sup>4</sup>*Department of Physics, University of Waterloo, Waterloo, On N2L 3G1, Canada*

## Abstract

We provide an asymptotically safe Pati-Salam embedding of the Standard Model. Safety is achieved by adding to the theory gauged vector-like fermions and by employing recently developed large number-of-flavor techniques and results. We show that the gauge, scalar quartic and Yukawa couplings achieve an interacting ultraviolet fixed point below the Planck scale. The minimal model is a relevant example of a Standard Model extension in which unification of *all* type of couplings occurs because of a dynamical principle, i.e. the presence of an ultraviolet fixed point. This extension differs from the usual Grand Unified Theories scenario in which only gauge couplings unify and become free with the remaining couplings left unsafe. We find renormalization group flow solutions that match the Standard Model couplings values at low energies allowing for realistic safe extensions of the Standard Model.

## 1 Introduction

The recent discovery of four dimensional asymptotically safe quantum field theories [1, 2] has opened the way to safe extensions of the Standard Model, starting with the envision of a *safe* rather than *free* QCD [3], to scenarios in which the gauge, the Yukawa and scalar quartic couplings are unified by a dynamical rather than a symmetry principle [5–8]. On the supersymmetric front, exact non perturbative results and constraints were first discussed coherently in [9], extending and correcting the results of [10] while opening the way to (non)perturbative supersymmetric safety in [11–13], and to the first applications for super GUT model building [11, 14]. Simultaneously there has been much advancement in our understanding of the nonsupersymmetric dynamics of large number of flavors gauge-Yukawa theories [15–19]. This has led, for example, to enrich the original conformal window [20, 21], reviewed in [22, 23], with a novel asymptotically safe region [24]. The discovery led to the upgraded *conformal window 2.0* of [24]. The large  $N_f$  dynamics of gauge-fermion theories has been extended to gauge-Yukawa theories starting with the Yukawa sector [25–27] and for the first time to all couplings in [28, 29]. A gauge-less study appeared in [30]. The results widened the palette of tools and theories at our disposal for novel large  $N_f$  safe extensions of the SM [7, 28, 31–33].

We use the acquired knowledge to construct a novel *safe Pati-Salam* extension by adding vector-like fermions and showing that all couplings acquire an UV fixed point at energies that are far from the onset of quantum gravity. The separation of scales allow us to investigate a condense-matter-like unification of the SM couplings before having to consider the gravitational corrections. The interplay with gravity has been investigated

in several recent works [34–38] and it will not be considered here. Differently from the usual Grand Unified scenarios [39] in which only the gauge couplings unify because of their embedding into a larger group structure and then they eventually become free, in the present scenario we have that Yukawa and scalar self couplings are intimately linked because of the safe dynamics with their high energy behavior tamed by the presence of an interacting fixed point.

The paper is organized as follows: In section 2 we review and introduce the Pati-Salam [40] extension of the SM and build the minimal vector-like structure able to support a safe scenario. We develop the renormalization group (RG) equations and determine the couplings' evolution in section 3. Here we analyze and classify the UV fixed point structure of the model. We discuss how to match the SM couplings at low energies in section 4. We offer our conclusions in section 5. In appendix A we summarize the one-loop RG equations for the Pati-Salam model investigated here.

## 2 Pati-Salam extension of the Standard Model

Consider the time-honored Pati-Salam gauge symmetry group  $G_{\text{PS}}$  [40]

$$G_{\text{PS}} = SU(4) \otimes SU(2)_L \otimes SU(2)_R, \quad (1)$$

with gauge couplings  $g_4$ ,  $g_L$  and  $g_R$ , respectively. Here the gauge group  $SU(4) \supset SU(3)_C \otimes U(1)_{B-L}$ , where  $SU(3)_C$  denotes the SM color gauge group, and the corresponding gauge couplings are related according to

$$g_3 = g_4, \quad g_{B-L} = \sqrt{\frac{3}{8}}g_3. \quad (2)$$

The gauge fields of  $G_{\text{PS}}$  can be written as follows:

$$\hat{W}_{L\mu} \equiv \frac{1}{2} \begin{pmatrix} W_{L\mu}^0 & \sqrt{2}W_{L\mu}^+ \\ \sqrt{2}W_{L\mu}^- & -W_{L\mu}^0 \end{pmatrix}, \quad (3)$$

$$\hat{W}_{R\mu} \equiv \frac{1}{2} \begin{pmatrix} W_{R\mu}^0 & \sqrt{2}W_{R\mu}^+ \\ \sqrt{2}W_{R\mu}^- & -W_{R\mu}^0 \end{pmatrix}, \quad (4)$$

$$\hat{G}_\mu \equiv \frac{1}{2} \begin{pmatrix} G_{3\mu} + \frac{G_{8\mu}}{\sqrt{3}} + \frac{B_\mu}{\sqrt{6}} & \sqrt{2}G_{12\mu}^+ & \sqrt{2}G_{13\mu}^+ & \sqrt{2}X_{1\mu}^+ \\ \sqrt{2}G_{12\mu}^- & -G_{3\mu} + \frac{G_{8\mu}}{\sqrt{3}} + \frac{B_\mu}{\sqrt{6}} & \sqrt{2}G_{23\mu}^+ & \sqrt{2}X_{2\mu}^+ \\ \sqrt{2}G_{13\mu}^- & \sqrt{2}G_{23\mu}^- & -\frac{2G_{8\mu}}{\sqrt{3}} + \frac{B_\mu}{\sqrt{6}} & \sqrt{2}X_{3\mu}^+ \\ \sqrt{2}X_{1\mu}^- & \sqrt{2}X_{2\mu}^- & \sqrt{2}X_{3\mu}^- & -\frac{3B_\mu}{\sqrt{6}} \end{pmatrix}. \quad (5)$$

In this parametrization,  $W_{L\mu}^0$  and  $W_{L\mu}^\pm$  correspond to the electroweak (EW) gauge bosons,  $G_{3\mu}$ ,  $G_{8\mu}$ ,  $G_{12\mu}^\pm$ ,  $G_{13\mu}^\pm$  and  $G_{23\mu}^\pm$  are the  $SU(3)_C$  gluons,  $B_\mu$  is the  $B-L$  gauge field, and  $X_{1\mu}^\pm$ ,  $X_{2\mu}^\pm$  and  $X_{3\mu}^\pm$  are leptoquarks.

The SM quark and lepton fields are unified into the  $G_{\text{PS}}$  irreducible representations

$$\begin{aligned} \psi_{Li} &= \begin{pmatrix} u_L & u_L & u_L & \nu_L \\ d_L & d_L & d_L & e_L \end{pmatrix}_i \sim (4, 2, 1)_i, \\ \psi_{Ri} &= \begin{pmatrix} u_R & u_R & u_R & \nu_R \\ d_R & d_R & d_R & e_R \end{pmatrix}_i \sim (4, 1, 2)_i, \end{aligned} \quad (6)$$

where  $i = 1, 2, 3$  is a flavor index.

In order to induce the breaking of  $G_{\text{PS}}$  to the SM gauge group, we introduce a scalar field  $\phi_R$  which transforms as the fermion multiplet  $\psi_R$ , that is  $\phi_R \sim (4, 1, 2)$ :

$$\phi_R = \begin{pmatrix} \phi_R^u & \phi_R^0 \\ \phi_R^d & \phi_R^- \end{pmatrix}, \quad (7)$$

where the neutral component  $\phi_R^0$  takes a non-zero vev,  $v_R \equiv \langle \phi_R^0 \rangle$ , such that  $G_{\text{PS}} \xrightarrow{v_R} SU(3)_C \otimes SU(2)_L \otimes U(1)_Y$ . The hypercharge  $Y$  is a linear combination between the diagonal generator of  $SU(2)_R$  and the generator of  $B - L$ , namely

$$Y = 2I_R + (B - L), \quad (8)$$

with  $\text{Tr}(I_R^2) = 1/2$  for the fundamental representation. Then, the EW gauge couplings  $g_2$  and  $g_Y$  result:

$$g_2 = g_L, \quad g_R = \frac{g_Y}{\sqrt{1 - 2g_Y^2/3g_3^2}}. \quad (9)$$

We also introduce an additional (complex) scalar field  $\Phi \sim (1, 2, 2)$ , with

$$\Phi = \begin{pmatrix} \phi_1^0 & \phi_2^+ \\ \phi_1^- & \phi_2^0 \end{pmatrix} \equiv (\Phi_1 \quad \Phi_2), \quad (10)$$

which is responsible of the breaking of the EW symmetry.

## 2.1 The Scalar sector

The general scalar potential of the model defined above is given by:

$$\begin{aligned} V(\Phi, \phi_R) = & -\mu_1^2 \text{Tr}(\Phi^\dagger \Phi) + \text{Re} \left[ \mu_{12}^2 \text{Tr}(\Phi^\dagger \Phi^c) \right] - \mu_R^2 \text{Tr}(\phi_R^\dagger \phi_R) \\ & + \lambda_1 \text{Tr}^2(\Phi^\dagger \Phi) + \text{Re} \left[ \lambda_2 \text{Tr}^2(\Phi^\dagger \Phi^c) \right] + \text{Re} \left[ \lambda_3 \text{Tr}(\Phi^\dagger \Phi) \text{Tr}(\Phi^\dagger \Phi^c) \right] \\ & + (\lambda_4 - 2\text{Re}\lambda_2) \left| \text{Tr}(\Phi^\dagger \Phi^c) \right|^2 \\ & + \lambda_{R1} \text{Tr}^2(\phi_R^\dagger \phi_R) + \lambda_{R2} \text{Tr}(\phi_R^\dagger \phi_R \phi_R^\dagger \phi_R) \\ & + \lambda_{R\Phi 1} \text{Tr}(\phi_R^\dagger \phi_R) \text{Tr}(\Phi^\dagger \Phi) + \text{Re} \left[ \lambda_{R\Phi 2} \text{Tr}(\phi_R \phi_R^\dagger) \text{Tr}(\Phi^\dagger \Phi^c) \right] \\ & + \lambda_{R\Phi 3} \text{Tr}(\phi_R^\dagger \phi_R \Phi^\dagger \Phi). \end{aligned} \quad (11)$$

The quartic couplings  $\lambda_{2,3}$  and  $\lambda_{R\Phi 2}$ , and the dimensional term  $\mu_{12}$ , carry a non-trivial phase in case CP symmetry is explicitly broken. We have also introduced the conjugate field  $\Phi^c \equiv \tau_2 \Phi^* \tau_2$ ,  $\tau_2$  being the standard Pauli matrix.

## 2.2 The Yukawa sector

The most general Yukawa Lagrangian for the matter fields  $\psi_{L/R}$  is <sup>1</sup>

$$\mathcal{L}_{\text{Yuk}}^\psi = y \text{Tr}[\overline{\psi}_L \Phi \psi_R] + y_c \text{Tr}[\overline{\psi}_L \Phi^c \psi_R] + \text{h.c.} \quad (12)$$

<sup>1</sup>We consider for simplicity only Yukawa couplings to the third fermion generation and we omit the flavor index  $i$  in  $\psi_{L/R}$ , see Eq. (6).

In terms of the SM fermion fields Eq. (12) reads:

$$\begin{aligned}
\mathcal{L}_{\text{Yuk}}^\psi = & y (\bar{t}_L t_R \phi_1^0 + \bar{t}_L b_R \phi_2^+ + \bar{b}_L t_R \phi_1^- + \bar{b}_L b_R \phi_2^0 \\
& + \bar{\nu}_L \nu_R \phi_1^0 + \bar{\nu}_L \tau_R \phi_2^+ + \bar{\tau}_L \nu_R \phi_1^- + \bar{\tau}_L \tau_R \phi_2^0) \\
& + y_c (\bar{t}_L t_R \phi_2^{0*} - \bar{t}_L b_R \phi_1^+ - \bar{b}_L t_R \phi_2^- + \bar{b}_L b_R \phi_1^{0*} \\
& + \bar{\nu}_L \nu_R \phi_2^{0*} - \bar{\nu}_L \tau_R \phi_1^+ - \bar{\tau}_L \nu_R \phi_2^- + \bar{\tau}_L \tau_R \phi_1^{0*}) + \text{h.c.}
\end{aligned} \tag{13}$$

Electroweak symmetry breaking is induced by a nonzero vev of  $\Phi$ , which takes the form:

$$\langle \Phi \rangle = \begin{pmatrix} u_1 & 0 \\ 0 & u_2 \end{pmatrix}, \tag{14}$$

with generally  $u_1 \neq u_2$ . From Eq. (13) we have the fermion mass spectrum:

$$\begin{aligned}
m_t = m_{\nu_\tau} &= (y \sin \beta + y_c \cos \beta)v, \\
m_b = m_\tau &= (y \cos \beta + y_c \sin \beta)v,
\end{aligned} \tag{15}$$

where  $v \equiv \sqrt{u_1^2 + u_2^2} = 174 \text{ GeV}$  and  $\tan \beta \equiv u_1/u_2$ . In the case of a self-conjugate bi-doublet field  $\Phi \equiv \Phi^c$ , one has  $u_1 = u_2$  in Eq. (14) and equality between fermion masses is enforced at tree-level, namely

$$m_t = m_b = m_\tau = m_{\nu_\tau}. \tag{16}$$

In order to separate the neutrino and top masses in Eq. (15) and Eq. (16) we implement the seesaw mechanism [41–44] by adding a new chiral fermion singlet  $N_L \sim (1, 1, 1)$ , which has Yukawa interaction

$$\mathcal{L}_{\text{Yuk}}^N = -y_\nu \bar{N}_L \text{Tr} [\phi_R^\dagger \psi_R] + \text{h.c.} \tag{17}$$

The latter generates a Dirac mass term  $M_R \bar{N}_L \nu_R$ , with  $M_R \equiv y_\nu v_R$ . The resulting Majorana mass term for the neutral fermion fields reads:

$$\mathcal{L}_{\text{mass}}^\nu = -\frac{1}{2} \begin{pmatrix} \bar{\nu}_R^c & \bar{\nu}_R & \bar{N}_R^c \end{pmatrix} \begin{pmatrix} 0 & m_t & 0 \\ m_t & 0 & M_R \\ 0 & M_R & 0 \end{pmatrix} \begin{pmatrix} \nu_L \\ \nu_L^c \\ N_L \end{pmatrix} + \text{h.c.} \tag{18}$$

with  $\nu_{L/R}^c \equiv C \bar{\nu}_{R/L}^T$  and  $N_R^c \equiv C \bar{N}_L^T$ . The mass spectrum consists of one massless neutrino

$$\nu_{\tau L} = -\cos \theta \nu_L + \sin \theta N_L, \tag{19}$$

with  $\tan \theta = m_t/M_R$ , and one Dirac neutrino  $N_D$  with mass  $m_D = \sqrt{m_t^2 + M_R^2}$  and chiral components:

$$\begin{aligned}
P_L N_D &= \nu_L \sin \theta + N_L \cos \theta, \\
P_R N_D &= \nu_R.
\end{aligned} \tag{20}$$

By adding a Majorana mass term for the singlet fermion  $N_L$

$$\mathcal{L}_{\text{mass}}^N = -\frac{1}{2} M_N \bar{N}_R^c N_L + \text{h.c.} \tag{21}$$

the total lepton number is explicitly broken and the spectrum consists of three massive neutrinos. Taking  $M_N \ll m_t, M_R$ , the mass eigenstates result in one light active Majorana neutrino  $\nu_\tau$  with mass

$$m_{\nu_\tau} = M_N \frac{m_t^2}{m_D^2} \quad (22)$$

and two quasi-degenerate heavy Majorana neutrinos  $N_{1,2}$  with opposite CP parities and masses

$$M_{1,2} = m_D \pm \frac{M_N}{2} \frac{M_R^2}{m_D^2}. \quad (23)$$

Threshold corrections may induce a sizable mass splitting between  $m_\tau$  and  $m_b$  in Eq. (15) and Eq. (16), which depends on the  $G_{PS}$  breaking scale  $v_R$ , see Ref. [45].

### 2.3 The minimal model

In the simplest scenario where the field  $\Phi$  is self-conjugate, the fermion spectrum is degenerate, see Eq. (16), and the scalar potential in Eq. (11) consists of the quartic couplings  $\lambda_1$ ,  $\lambda_{R1,2}$  and  $\lambda_{R\Phi 1,3}$ . As discussed above, by adding a new chiral fermion  $N_L$ , which is a singlet under  $G_{PS}$ , it is possible to induce a hierarchy between the top quark and neutrino masses via the seesaw mechanism, such that the correct light neutrino mass scale can be accommodated. Here, we further extend the matter content of the theory with a new vector-like fermion  $F \sim (10, 1, 1)$  with mass  $M_F$  and Yukawa interactions:

$$\mathcal{L}_{\text{Yuk}}^F = y_F \text{Tr} (\overline{F}_L \phi_R^T i\tau_2 \psi_R) + \text{h.c.} \quad (24)$$

In terms of the  $SU(3)_C$  representations, the field  $F$  can be decomposed as

$$F = \begin{pmatrix} S & B\sqrt{2} \\ B^T\sqrt{2} & E \end{pmatrix}, \quad (25)$$

where  $S$ ,  $B$  and  $E$  denote a color sextet, triplet and singlet, respectively. Then, from Eq. (24) the fields  $B$  and  $E$  mix with the right-handed components of  $\psi_R$ ,  $b_R$  and  $\tau_R$ , respectively, giving the overall Dirac mass terms:

$$\mathcal{L}_{\text{mass}}^b = (\overline{b}_L \quad \overline{B}_L) \begin{pmatrix} m_t & 0 \\ m_B & M_F \end{pmatrix} \begin{pmatrix} b_R \\ B_R \end{pmatrix} + \text{h.c.}, \quad (26)$$

$$\mathcal{L}_{\text{mass}}^\tau = (\overline{\tau}_L \quad \overline{E}_L) \begin{pmatrix} m_t & 0 \\ \sqrt{2}m_B & M_F \end{pmatrix} \begin{pmatrix} \tau_R \\ E_R \end{pmatrix} + \text{h.c.}, \quad (27)$$

with  $m_B \equiv y_F v_R / \sqrt{2}$ . As a result of this mixing, the top quark becomes naturally heavier than the other SM fermions. In fact, in the limit  $m_B \gg m_t, M_F$ , the  $b$  quark and  $\tau$  charged lepton masses satisfy the tree-level relation:

$$m_b = \sqrt{2} m_\tau \approx \frac{M_F m_t}{\sqrt{2} m_B}. \quad (28)$$

Analogously, we have a new vector-like quark,  $\hat{B}$ , and a new vector-like lepton,  $\hat{E}$ , with corresponding masses  $M_B$  and  $M_E$ , which satisfy the tree-level relation:

$$M_B = M_E / \sqrt{2} \approx m_B. \quad (29)$$

Gauge Couplings	Yukawa Couplings	Scalar Couplings
$SU(4) : g_4$	$\psi_{L/R} : y, y_c$	$\phi_R : \lambda_{R1}, \lambda_{R2}$
$SU(2)_L : g_L$	$N_L : y_\nu$	portal: $\lambda_{R\Phi_1}, \lambda_{R\Phi_2}, \lambda_{R\Phi_3}$
$SU(2)_R : g_R$	$F : y_F$	$\Phi : \lambda_1, \lambda_2, \lambda_3, \lambda_4$

Table 1: Gauge, Yukawa and scalar quartic couplings of the Pati-Salam model.

### 3 Renormalization group analysis

In this section, we perform the RG analysis of the Pati-Salam extension of the SM introduced above and discuss the relevant phenomenological implications. The gauge, Yukawa and scalar couplings in the minimal and extended realizations are listed in Tab. 1. The corresponding RG equations at one loop order are reported in appendix A.

#### 3.1 Large- $N$ beta function

In order to ensure asymptotic safety in the UV for all the system in Tab. 1, we employ the  $1/N_F$  expansion approach developed in [15–17, 46], first applied to the whole SM in [31]. More specifically, we introduce  $N_F \gg 1$  vector-like fermions, which transform non-trivially under  $G_{\text{PS}}$ . In this framework, the RG equations receive a contribution at leading order in the  $1/N_F$  expansion of the relevant Feynman diagrams, which are resummed as shown in Fig 1 (only gauge coupling cases are shown). This non-perturbative effect induces an interacting fixed point for both the Abelian and non-Abelian gauge interactions of the SM [31]. The fixed point is guaranteed by the pole structure occurred in the expressions of the summation [16, 17].

In the present scenario, we consider three sets of vector-like fermions charged under  $G_{\text{PS}}$ , with the following charge assignment:

$$N_{F_4} (4, 1, 1) \oplus N_{F_{2L}} (1, 3, 1) \oplus N_{F_{2R}} (1, 1, 2) , \quad (30)$$

where the  $N_{F_{2L}}$  vector-like fermions are chosen in the adjoint representation of  $SU(2)_L$  to avoid fractional electrical charges. We have also chosen each set of vector-like fermions to have non-trivial charges only under one simple gauge group to avoid the extra contributions in the summation of semi-simple group.

#### 3.2 Large- $N$ gauge beta function and gauge coupling unification

To the leading  $1/N_F$  order for each set, the higher order (ho) contributions (i.e. the bubble diagrams in Fig. 1) to the RG functions of the gauge couplings are calculated in [17], while for the abelian case they were first computed in [15]. Here we list a short summary of the results. The higher order contributions are give by:

$$\beta_i^{\text{ho}} = \frac{2A_i\alpha_i}{3} \frac{H_{1_i}(A_i)}{N_{F_i}}, \quad \alpha_i \equiv \frac{g_i^2}{(4\pi)^2} \quad (i = 2L, 2R, 4) , \quad (31)$$

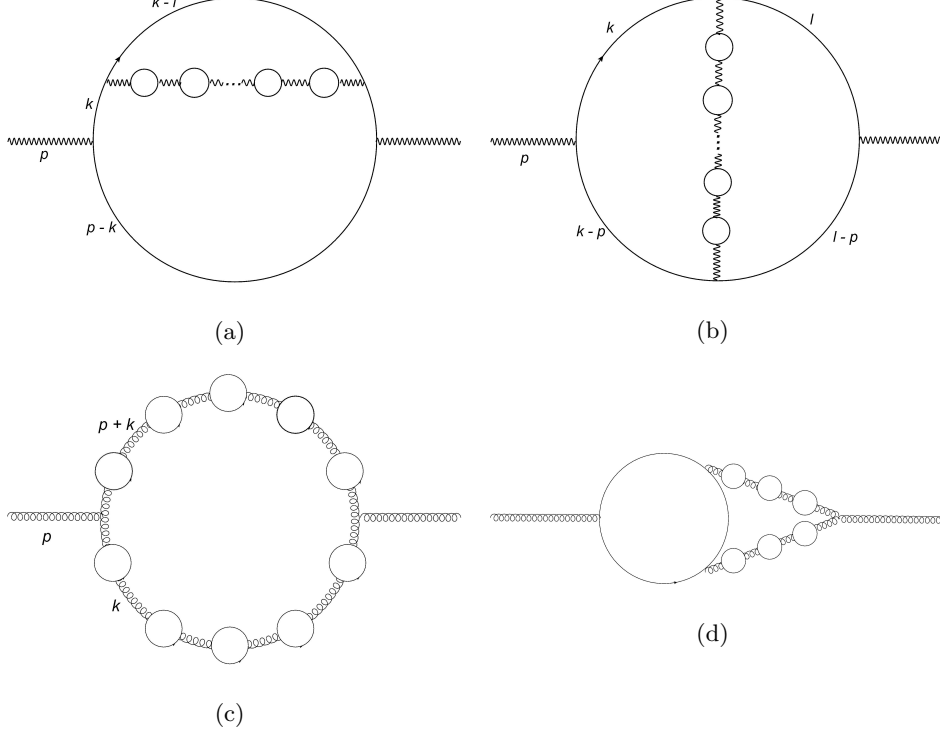


Figure 1: Feynman diagrams for gauge field renormalization at order  $1/N_F$ . Diagrams (a) and (b) are present in both the Abelian and non-Abelian 2-point functions, while (c) and (d) only exist in the non-Abelian theory.

with the functions  $H_{1i}$  and the t'Hooft couplings  $A_i$  given by

$$\begin{aligned}
A_i &= 4\alpha_i T_R N_{F_i} \\
H_{1_i} &= \frac{-11}{2} N_{ci} + \int_0^{A_i/3} I_1(x) I_2(x) dx \quad (N_{ci} = 2, 4) \\
I_1(x) &= \frac{(1+x)(2x-1)^2(2x-3)^2 \sin(\pi x)^3}{(x-2)\pi^3} \times \left( \Gamma(x-1)^2 \Gamma(-2x) \right) \\
I_2(x) &= \frac{N_{ci}^2 - 1}{N_{ci}} + \frac{(20 - 43x + 32x^2 - 14x^3 + 4x^4)}{2(2x-1)(2x-3)(1-x^2)} N_{ci}.
\end{aligned} \tag{32}$$

The Dynkin indices are  $T_R = 1/2 (N_{ci})$  for the fundamental (adjoint) representation. The RG functions of the gauge couplings (see Appendix A) including the contributions of bubble diagrams resummation are listed below:

$$\begin{aligned}
\beta_{\alpha_{2L}}^{tot} &= \frac{d\alpha_{2L}}{d \log \mu} = \beta_{\alpha_{2L}}^{1loop} + \beta_{\alpha_{2L}}^{ho} = -6\alpha_{2L}^2 + \frac{2A_{2L}\alpha_{2L}}{3} \frac{H_{1_{2L}}(A_{2L})}{N_{F_{2L}}} \\
\beta_{\alpha_{2R}}^{tot} &= \frac{d\alpha_{2R}}{d \log \mu} = \beta_{\alpha_{2R}}^{1loop} + \beta_{\alpha_{2R}}^{ho} = -\frac{14}{3}\alpha_{2R}^2 + \frac{2A_{2R}\alpha_{2R}}{3} \frac{H_{1_{2R}}(A_{2R})}{N_{F_{2R}}} \\
\beta_{\alpha_4}^{tot} &= \frac{d\alpha_4}{d \log \mu} = \beta_{\alpha_4}^{1loop} + \beta_{\alpha_4}^{ho} = -18\alpha_4^2 + \frac{2A_4\alpha_4}{3} \frac{H_{1_4}(A_4)}{N_{F_4}},
\end{aligned} \tag{33}$$

where the  $\beta_{\alpha_{2L}}^{1loop}$ ,  $\beta_{\alpha_{2R}}^{1loop}$ ,  $\beta_{\alpha_4}^{1loop}$  are denoted as the original one loop RG beta functions of the three gauge couplings without bubble diagram contributions while  $\beta_{\alpha_{2L}}^{tot}$ ,  $\beta_{\alpha_{2R}}^{tot}$ ,  $\beta_{\alpha_4}^{tot}$

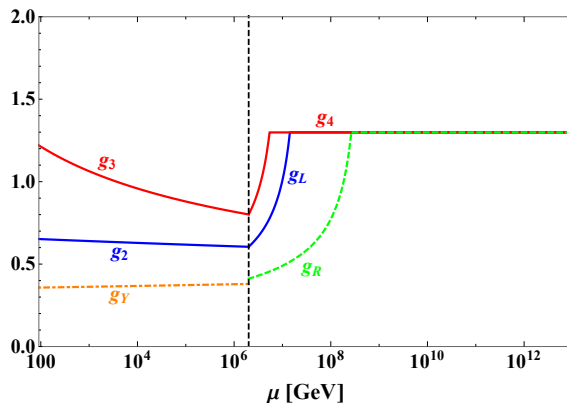


Figure 2: We show a sample case of gauge unification, where we have chosen  $N_{F_{2L}} = 35$ ,  $N_{F_{2R}} = N_{F_4} = 140$ . The dashed line represents the Pati-Salam symmetry breaking scale at 2000 TeV where all the vector-like fermions are introduced. The three couplings  $g_Y$ ,  $g_2$ ,  $g_3$  at the left hand side of the dashed line are determined by the running of the SM gauge couplings.

are the total RG beta functions including the higher order bubble diagram contributions up to  $1/N_F$  order. The reason that only one loop RG beta functions of the gauge couplings are used will be clear later on.

Thus, the UV fixed point for the gauge coupling sub-system ( $g_4$ ,  $g_L$ ,  $g_R$ ) is guaranteed by the pole structure in the bubble diagram summation. For all the non-abelian gauge groups, the pole in the function  $H_{1_i}$ , and thus the UV fixed point of the non-abelian gauge couplings, always occurs at  $A_i = 3$ . In particular, if one chooses the vector-like fermion representation with  $A_{2L} = A_{2R} = A_4$ , gauge coupling unification is guaranteed. This is shown in Fig. 5, where we set  $N_{F_{2L}} = 35$  and  $N_{F_{2R}} = N_{F_4} = 140$ . The IR initial conditions of  $g_L$ ,  $g_R$  and  $g_4$  are obtained by using the matching conditions of Eq. (2) and Eq. (9) and the SM couplings are running from the EW scale to the Pati-Salam symmetry breaking scale. For simplicity, we have assumed all the vector-like fermions were introduced at the Pati-Salam symmetry breaking scale  $v_R$ . The latter is most strongly constrained by the kaon decay  $K_L \rightarrow \mu^\pm e^\mp$  (see e.g. [45, 47]). Using the current upper limit  $\text{Br}(K_L \rightarrow \mu^\pm e^\mp) < 4.7 \times 10^{-12}$  provided in [48], we obtain the lower limit  $v_R \gtrsim 2000$  TeV (see also e.g. [49]). In order to make closer connection to low energy phenomenology, in this work we choose the Pati-Salam symmetry breaking scale exactly at 2000 TeV.

### 3.3 Large- $N$ Yukawa and quartic beta function

In the previous section, we have only considered the bubble diagram contributions in the gauge couplings subsystem. However, the bubble diagrams can directly contribute also to the quartic and Yukawa beta functions (see e.g. [25, 29]). In the following, we provide a brief review of the procedure following [29].

The bubble diagram contributions to known 1-loop beta functions of quartic and Yukawa couplings can be obtained by employing the following recipe. The Yukawa beta



function at large number of fermions can be written in the compact form

$$\beta_y = c_1 y^3 + y \sum_{\alpha} c_{\alpha} g_{\alpha}^2 I_y(A_{\alpha}), \quad \text{with}$$

$$I_y(A_{\alpha}) = H_{\phi}\left(0, \frac{2}{3}A_{\alpha}\right) \left(1 + A_{\alpha} \frac{C_2(R_{\phi}^{\alpha})}{6\left(C_2(R_{\chi}^{\alpha}) + C_2(R_{\xi}^{\alpha})\right)}\right) \quad (34)$$

$$H_{\phi}(x) = H_0(x) = \frac{(1 - \frac{x}{3})\Gamma(4-x)}{3\Gamma^2(2 - \frac{x}{2})\Gamma(3 - \frac{x}{2})\Gamma(1 + \frac{x}{2})}$$

containing information about the resummed fermion bubbles and  $c_1, c_{\alpha}$  are the standard 1-loop coefficients for the Yukawa beta function while  $C_2(R_{\phi}^{\alpha}), C_2(R_{\chi}^{\alpha}), C_2(R_{\xi}^{\alpha})$  are the Casimir operators of the corresponding scalar and fermion fields. Thus, when  $c_1, c_{\alpha}$  are known, the full Yukawa beta function including the bubble diagram contributions can be obtained. Similarly, for the quartic coupling we write

$$\beta_{\lambda} = c_1 \lambda^2 + \lambda \sum_{\alpha} c_{\alpha} g_{\alpha}^2 I_{\lambda g^2}(A_{\alpha}) + \sum_{\alpha} c'_{\alpha} g_{\alpha}^4 I_{g^4}(A_{\alpha}) + \sum_{\alpha < \beta} c_{\alpha\beta} g_{\alpha}^2 g_{\beta}^2 I_{g_1^2 g_2^2}^{tot}(A_{\alpha}, A_{\beta}), \quad (35)$$

with  $c_1, c_{\alpha}, c'_{\alpha}, c_{\alpha\beta}$  the known 1-loop coefficients for the quartic beta function and the resummed fermion bubbles appear via

$$I_{\lambda g^2}(K_{\alpha}) = H_{\phi}\left(0, \frac{2}{3}A_{\alpha}\right)$$

$$I_{g^4}(K_{\alpha}) = H_{\lambda}\left(1, \frac{2}{3}A_{\alpha}\right) + A_{\alpha} \frac{dH_{\lambda}\left(1, \frac{2}{3}A_{\alpha}\right)}{dA_{\alpha}}$$

$$I_{g_1^2 g_2^2}^{tot}(A_{\alpha}, A_{\beta}) = \frac{1}{3} \left[ I_{g_1^2 g_2^2}(A_{\alpha}, 0) + I_{g_1^2 g_2^2}(0, A_{\beta}) + I_{g_1^2 g_2^2}(A_{\alpha}, A_{\beta}) \right] \quad (36)$$

$$I_{g_1^2 g_2^2}(A_{\alpha}, A_{\beta}) = \frac{1}{A_{\alpha} - A_{\beta}} \left[ A_{\alpha} H_{\lambda}\left(1, \frac{2}{3}A_{\alpha}\right) - A_{\beta} H_{\lambda}\left(1, \frac{2}{3}A_{\beta}\right) \right], \quad \text{where}$$

$$H_{\lambda}(1, x) = (1 - \frac{x}{4})H_0(x) = \frac{(1 - \frac{x}{4})(1 - \frac{x}{3})\Gamma(4-x)}{3\Gamma^2(2 - \frac{x}{2})\Gamma(3 - \frac{x}{2})\Gamma(1 + \frac{x}{2})}.$$

Thus we have now the full quartic beta function including the bubble diagram contributions when  $c_1, c_{\alpha}, c'_{\alpha}, c_{\alpha\beta}$  are known. Following the above recipe, the bubble diagram improved Yukawa beta function  $\beta_y$ , for example, can be written as

$$(4\pi)^2 \beta_y = \left( -\frac{9}{4} g_L^2 I_y(A_L) - \frac{45}{4} g_4^2 I_y(A_4) - \frac{9}{4} g_R^2 I_y(A_R) + 20y_c^2 + y_{\nu}^2 \right) y + 12y^3. \quad (37)$$

The bubble diagram improved quartic beta function  $\beta_{\lambda_{R1}}$  reads

$$(4\pi)^2 \beta_{\lambda_{R1}} = 192\lambda_{R1}^2 + \lambda_{R1} \left( -\frac{45}{2} g_4^2 I_{\lambda g^2}(A_4) - 9g_R^2 I_{\lambda g^2}(A_R) + 192\lambda_{R2} + 8y_{\nu}^2 \right)$$

$$+ \frac{27}{32} g_4^2 g_R^2 \times \frac{1}{3} \left( I_{g_1^2 g_2^2}(A_4, A_R) + I_{g_1^2 g_2^2}(0, A_R) + I_{g_1^2 g_2^2}(A_4, 0) \right) \quad (38)$$

$$+ \frac{27}{128} g_4^4 I_{g^4}(A_4) + \frac{9}{32} g_R^4 I_{g^4}(A_R) + 48\lambda_{R2}^2 + 16\lambda_{R\Phi 1}^2 - 2y_{\nu}^4.$$

### 3.4 UV fixed point solutions in the gauge-Yukawa-quartic system

To prove the existence of a fixed point of the whole system in Tab. 1, we are entitled to assume the gauge couplings at the UV fixed point as background values (i.e. constants

$\lambda_1$	$\lambda_2$	$\lambda_3$	$\lambda_4$	$\lambda_{R\Phi_1}$	$\lambda_{R\Phi_{2,3}}$	$\lambda_{R1}$	$\lambda_{R2}$	$y$	$y_c$	$y_\nu$	$y_F$
0.12	0.05	0	0.13	0.02	0	0.13	-0.01	0.78	0.78	0.84	0

Table 2: This table summarizes the sample UV fixed point solution with sample value ( $N_{F_{2L}} = 40$ ,  $N_{F_{2R}} = 150$ ,  $N_{F_4} = 200$ ) involving the bubble diagram contributions in the Yukawa and quartic RG beta functions.

$\lambda_1$	$\lambda_2$	$\lambda_3$	$\lambda_4$	$\lambda_{R\Phi_1}$	$\lambda_{R\Phi_{2,3}}$	$\lambda_{R1}$	$\lambda_{R2}$	$y$	$y_c$	$y_\nu$	$y_F$
0.21	0.07	0	0.24	0.03	0	0.27	-0.02	1.05	1.05	1.19	0

Table 3: This table summarizes the UV fixed point solution for ( $N_{F_{2L}} = 40$ ,  $N_{F_{2R}} = 80$ ,  $N_{F_4} = 100$ ) involving the bubble diagram contributions in the Yukawa and quartic RG beta functions.

$\lambda_1$	$\lambda_2$	$\lambda_3$	$\lambda_4$	$\lambda_{R\Phi_1}$	$\lambda_{R\Phi_{2,3}}$	$\lambda_{R1}$	$\lambda_{R2}$	$y$	$y_c$	$y_\nu$	$y_F$
0.05	0.02	0	0.01	0.04	0	0.02	0.08	0.24	0.24	0.57	0.74

Table 4: This table summarizes the UV fixed point solution for ( $N_{F_{2L}} = 40$ ,  $N_{F_{2R}} = 130$ ,  $N_{F_4} = 130$ ) involving the bubble diagram contributions in the Yukawa and quartic RG beta functions.

in the RG functions of other couplings). This is so because at the UV fixed point they only depend on the choice of  $N_F$ . By using the one loop RG functions in appendix A augmented with the large- $N$  corrections (i.e. Eq. (34) and Eq. (35)), we can now set  $\{\beta_i = 0\}$  where  $i$  denotes all the Yukawa and scalar couplings presented in Tab. 1. Our investigation and beta functions are consistent with the large- $N$  limit, computations and results established in [29, 31].

We impose CP invariance, that implies:  $\text{Im}(\lambda_2) = \text{Re}(\lambda_3) = \text{Re}(\lambda_{R\Phi_2}) = 0$ . This symmetry requires  $y = \pm y_c$ , leading to top and bottom mass degeneracy, which is lifted when including the new vector-like fermion  $F \sim (10, 1, 1)$  (see Eq. (24)). We have also checked that, when breaking the CP symmetry safety is lost, because the overall RG system is over-constrained.

The analysis unveils several UV candidate fixed points for different choices of  $N_F$ . For example, for  $N_{F_{2L}} = 40$ ,  $N_{F_{2R}} = 150$ ,  $N_{F_4} = 200$ , we discover 30 sets of UV candidate fixed point. However the scalar potential is unbounded for several candidates UV fixed points. We therefore require the following vacuum stability conditions (see e.g. [50]) to be satisfied:

$$\lambda_{R1} + \lambda_{R2} > 0 \quad \lambda_1 - \lambda_2 + \lambda_4 > 0, \quad \lambda_1 > 0. \quad (39)$$

These conditions are quite constraining, reducing to 5 the original set of 30 UV fixed point candidates.

Consider the same value of the number of vector-like fermions discussed above (i.e.  $N_{F_{2L}} = 40$ ,  $N_{F_{2R}} = 150$ ,  $N_{F_4} = 200$ ). We now select one sample UV fixed point solutions summarized in Tab. 2. The solutions listed in Tab. 2 satisfy the vacuum stability condition Eq. (39). For a different sample value of the number of vector-like fermions ( $N_{F_{2L}} = 40$ ,  $N_{F_{2R}} = 80$ ,  $N_{F_4} = 100$ ), we also find a set of UV fixed point solutions which satisfy the vacuum stability conditions (see Tab. 3).

So far  $y_F$  was asymptotically free (see Tab. 2 and Tab. 3,) and we now exhibit the case in which  $y_F \neq 0$  in the UV. This case is shown in Tab. 4 in which we have a UV safe solution for  $y_F$  for ( $N_{F_{2L}} = 40$ ,  $N_{F_{2R}} = 130$ ,  $N_{F_4} = 130$ ). Interestingly this solution owes its existence to the bubble diagram contributions for the Yukawa and quartic RG beta functions. Thus, the large- $N$  contributions for the Yukawa and quartic couplings add novel safe possibilities in which all Yukawa couplings are safe.

	$\lambda_1$	$\lambda_2$	$\lambda_3$	$\lambda_4$	$\lambda_{R\Phi_1}$	$\lambda_{R\Phi_2}$	$\lambda_{R\Phi_3}$	$\lambda_{R1}$	$\lambda_{R2}$	$y$	$y_c$	$y_\nu$	$y_F$
1	Irev	×	×	×	Rev	Rev	×	Irev	Rev	Irev	Irev	Irev	0
2	Rev	×	×	Irev	Irev	Rev	×	Irev	Rev	Irev	Irev	Irev	0
3	Irev	Rev	×	×	Rev	Irev	×	Irev	Rev	Irev	Irev	Irev	0
4	Irev	Rev	0	Irev	Irev	0	0	Irev	Rev	Irev	Irev	Irev	0
5	Irev	Rev	0	Irev	Irev	0	0	Irev	Irev	Irev	Irev	Irev	Irev

Table 5: Classifications of the UV fixed point solutions of the couplings with relevant (Rev) and irrelevant (Irev) characteristics are listed. The symbol “ $\times$ ” denotes the corresponding coupling is turned off for simplification. From scenario 1 to 5, the complication of the scenario is gradually increased.  $y_F = 0$  is due to the asymptotically free solution we choose while  $\lambda_3$ ,  $\lambda_{R\Phi_2}$  and  $\lambda_{R\Phi_3}$  are chosen to be zero at all scale for simplification.

We now determine which fixed point is relevant/irrelevant (UV repulsive/attractive) following the convention according to which the RG flows towards the IR. The results are summarized in Tab. 5. We consider the cases that abide the vacuum stability conditions. We use “ $\times$ ” to represent that the couplings are turned off to simplify the system. We gradually increase the complexity of the system from scenario 1 to 5 where more and more couplings are involved. Scenario 4 (two sample cases, for example, will be the BF row and AF row in Tab. 2) and scenario 5 (one sample case will be the AF row in Tab. 4) possess all the couplings involved in our Pati-Salam model. The value 0 denotes a zero value solution at the fixed point. There are two distinct cases in which a specific coupling can be zero at the UV fixed point: the coupling can be asymptotically free or can vanish at all scales. For example,  $y_F$  is asymptotically free and therefore it leads to interesting physics in the IR while  $\lambda_3$ ,  $\lambda_{R\Phi_2}$  and  $\lambda_{R\Phi_3}$  can be set to zero at all energies, with the current approximations. This is what is assumed in the last row of Tab. 5 to simplify the analysis.

We employed two approaches to determine the RG flow of the system: the IR to UV approach and the UV to IR approach. In the IR to UV approach, the RG flow of the irrelevant couplings is constrained on certain trajectories, the separatrices.<sup>2</sup> Thus, we can solve the set of equations  $\beta_i = 0$  ( $i$  corresponding to all the irrelevant couplings) and solve for all the irrelevant couplings as function of the relevant couplings. The IR initial conditions of the relevant couplings are compatible with the phenomenological constraints while preserving UV safety. For the UV to IR approach one simply starts from the UV fixed point and attempts to run towards the IR. Here we use the fact that the gauge couplings have RG functions that are sufficiently decoupled from the other couplings. Thus, we can run the remaining couplings along the determined gauge coupling RG trajectories.

We report our results in Figs. 3 and 4 where we show the running of the gauge, Yukawa and scalar couplings by using the UV to IR approach for ( $N_{F_{2L}} = 40$ ,  $N_{F_{2R}} = 130$ ,  $N_{F_4} = 130$ ). The corresponding UV fixed point solution is the one shown in the AF row of Tab. 4. As mentioned above the RG flows of the gauge couplings are determined once the IR conditions are given. The IR initial conditions for  $g_L$ ,  $g_R$  and  $g_4$  are obtained by using the matching conditions of Eq. (2) and Eq. (9) and the SM couplings are running from the EW scale to the Pati-Salam symmetry breaking scale. For simplicity, the vector-like fermions masses are taken to be the Pati-Salam symmetry breaking scale  $v_R = 2000$  TeV. From Figs. 3 and 4, it is clear that all couplings (i.e. gauge, Yukawa and scalar quartic) achieve a safe UV fixed point. The transition scale, above which,

<sup>2</sup>A separatrix is the globally defined trajectory dividing the RG flow into distinct physical regions.

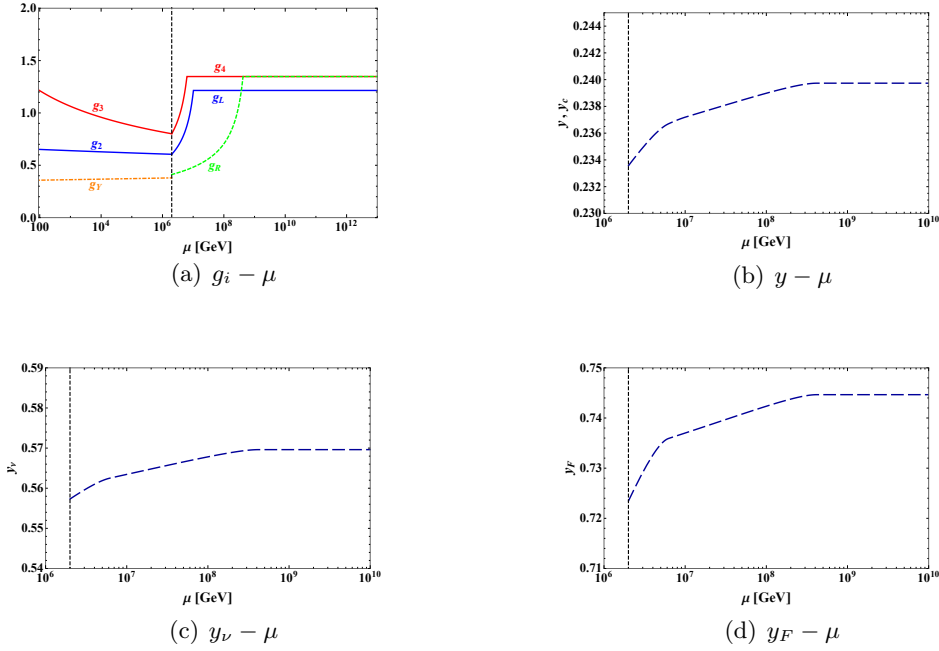


Figure 3: RG running of the gauge and Yukawa couplings by using the UV to IR approach. We have chosen  $N_{F2} = 40$ ,  $N_{F3} = 130$ ,  $N_{F4} = 130$ . We have used the matching conditions at IR (see Eq. (2) and Eq. (9)) to set the initial conditions of  $g_L$ ,  $g_R$ ,  $g_4$  at IR. For simplification, we have assumed that the vector-like fermions under gauge different symmetry groups are exactly introduced at the Pati-Salam breaking scale,  $v_R = 2000$  TeV, marked by a vertical dashed line.

the UV fixed point is reached is about  $0.5 \times 10^9$  GeV for all the couplings. Note that we could shift this transition scale significantly by increasing (the scale will decrease) or decreasing (the scale will increase) the number of vector-like fermions.

## 4 Matching the Standard Model

We now consider gluing the ultraviolet safe theory to the SM couplings at low energies, which is an important test in order to render our high energy safe extension phenomenologically viable. We start with the scalar component of the theory.

### 4.1 Scalar Sector

After Pati-Salam symmetry breaking, the scalar bi-doublet should match the conventional two Higgs doublet model which is defined by the Lagrangian:

$$\begin{aligned}
V_H = & m_{11}^2 \Phi_1^\dagger \Phi_1 + m_{22}^2 \Phi_2^\dagger \Phi_2 - \left( m_{12}^2 \Phi_1^\dagger \Phi_2 + \text{H.c.} \right) \\
& + \bar{\lambda}_1 \left( \Phi_1^\dagger \Phi_1 \right)^2 + \bar{\lambda}_2 \left( \Phi_2^\dagger \Phi_2 \right)^2 + \bar{\lambda}_3 \left( \Phi_1^\dagger \Phi_1 \right) \left( \Phi_2^\dagger \Phi_2 \right) + \bar{\lambda}_4 \left( \Phi_1^\dagger \Phi_2 \right) \left( \Phi_2^\dagger \Phi_1 \right) \\
& + \left[ \frac{1}{2} \bar{\lambda}_5 \left( \Phi_1^\dagger \Phi_2 \right)^2 + \bar{\lambda}_6 \left( \Phi_1^\dagger \Phi_1 \right) \left( \Phi_1^\dagger \Phi_2 \right) + \bar{\lambda}_7 \left( \Phi_2^\dagger \Phi_2 \right) \left( \Phi_1^\dagger \Phi_2 \right) + \text{H.c.} \right].
\end{aligned} \tag{40}$$

Comparing (40) with (11), we find:

$$\begin{aligned}
\bar{\lambda}_1 = \lambda_1, \quad \bar{\lambda}_2 = \lambda_1, \quad \bar{\lambda}_3 = 2\lambda_1, \quad \bar{\lambda}_4 = 4(-2\lambda_2 + \lambda_4) \\
\bar{\lambda}_5 = 4\lambda_2, \quad \bar{\lambda}_6 = -\lambda_3, \quad \bar{\lambda}_7 = \lambda_3.
\end{aligned} \tag{41}$$

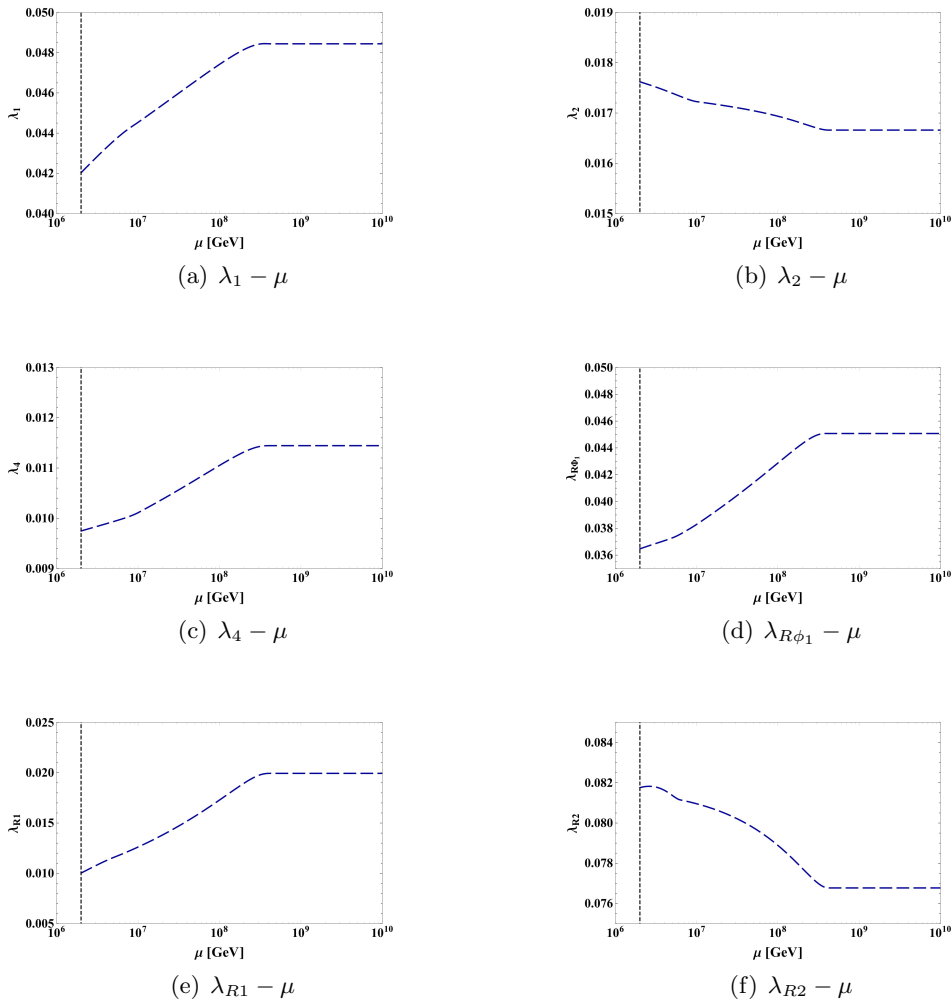


Figure 4: RG running of the scalar quartic couplings using the UV to IR approach for  $N_{F2} = 40$ ,  $N_{F3} = 130$ ,  $N_{F4} = 130$ . All the vector-like fermions appear (dashed line) at the symmetry breaking scale of the Pati-Salam group, which is around 2000 TeV.

When a set of  $(N_{F2}, N_{F3}, N_{F4})$  is given and a Pati-Salam symmetry breaking pattern is chosen, by using the RG running from a specific UV fixed point, we could predict the coupling values at the Pati-Salam symmetry breaking scale. After implementing the matching conditions of Eq. (41) these couplings become our new initial values so that by employing the two Higgs doublet RG beta functions [55], we could obtain the coupling values at the electroweak scale.

At this point we turn our attention to the mass matrix (neutral scalar fields) of the two Higgs doublet model:

$$M_{\text{neutral}}^2 = \begin{bmatrix} \frac{m_{12}^2 v_2}{v_1} + 2\bar{\lambda}_1 v_1^2 & -m_{12}^2 + (\bar{\lambda}_3 + \bar{\lambda}_4 + \bar{\lambda}_5) v_1 v_2 \\ -m_{12}^2 + (\bar{\lambda}_3 + \bar{\lambda}_4 + \bar{\lambda}_5) v_1 v_2 & \frac{m_{12}^2 v_2}{v_1} + 2\bar{\lambda}_2 v_2^2 \end{bmatrix}. \quad (42)$$

Note that this mass matrix is defined at the electroweak scale and to make sure that the computation is complete, we further included the higher order corrections for the mass matrix (e.g. the RG improved mass matrix), which for simplicity are not shown explicitly in Eq. (42). By using the coupling values obtained previously at the electroweak scale,

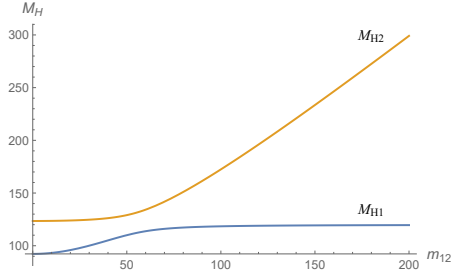


Figure 5: In this figure, we show two mass eigenvalues of the CP-even neutral Higgs mass matrix as a function of  $m_{12}$ .  $M_{H1}$  denotes the lighter Higgs while  $M_{H2}$  denotes the heavier one.

we determine the mass eigenvalues. The important phenomenological constraints are: both eigenvalues of the mass matrix should be positive and the lighter one should be close to the 125 GeV value of the observed Higgs mass. It can be shown that by choosing  $N_{F2} = 32$ ,  $N_{F3} = 108$ ,  $N_{F4} = 56$ , we obtain the following coupling values at around the electroweak scale:

$$\bar{\lambda}_1 = 0.222, \bar{\lambda}_2 = 0.222, \bar{\lambda}_3 = 0.250, \bar{\lambda}_4 = -0.380, \bar{\lambda}_5 = 0.260, y = 0.614. \quad (43)$$

It is interesting to discuss two cases in the following: the one for which we set  $m_{12} = 0$  and the other for  $m_{12} \neq 0$ . For the case with  $m_{12} = 0$ , we obtain two neutral scalar masses, one with  $\sim 92$  GeV (lighter Higgs) and an heavier one of  $\sim 123$  GeV. We stress that the choice ( $N_{F2} = 32$ ,  $N_{F3} = 108$ ,  $N_{F4} = 56$ ) is among the ones in which one can achieve the heaviest Higgs mass. We find intriguing that to push the lighter Higgs to be closer to the observed Higgs mass requires the Pati-Salam symmetry breaking scale not to be too far away from  $10^4$  TeV. Overall, for  $m_{12} = 0$ , both mass eigenvalues are phenomenologically too light. For the case with  $m_{12} \neq 0$ , we find both mass eigenvalues to increase when increasing  $m_{12}$ . In particular the light Higgs for the above choice of  $N_F$  seems to converge towards the value of 120 GeV (almost not changing after  $m_{12} > 150$  GeV) while the heavier Higgs mass keeps increasing with  $m_{12}$ . When choosing  $m_{12} = 150$  GeV, the light Higgs and the heavy Higgs masses are respectively 120 GeV and 264 GeV. We find that also in this case, there is a constraint on the Pati-Salam symmetry breaking scale. Slightly different from the case where  $m_{12} = 0$ , it now requires the Pati-Salam symmetry breaking scale to be larger than  $10^4$  TeV in order to yield a phenomenologically viable Higgs mass.

We also found alternative RG flow solutions leading to two light Higgs (we briefly list the result here). For  $N_{F2} = 36$ ,  $N_{F3} = 109$ ,  $N_{F4} = 118$ , we could have one light Higgs at 22.6 GeV and the heavy one at 125 GeV. We point to recent studies in the detection of light scalars [56][57].

## 4.2 Yukawa Sector

The top Yukawa mass term by using Eq. (15) at the electroweak scale is given by :

$$m_{\text{top}} = (y \sin \beta + y_c \cos \beta)v = \sqrt{2}yv, \quad (44)$$

where we have implemented the CP symmetry leading to  $y = y_c$  and  $\tan \beta = 1$ . Thus it is clear that to obtain the correct top quark mass at the electroweak scale,  $y$  should be  $\sim \frac{0.93}{\sqrt{2}} \sim 0.66$  which is smaller than the conventional SM top Yukawa coupling value. From Eq. (43), we obtain  $y = 0.614$  which is close to the required value.

To obtain the correct bottom quark mass, we have discussed previously that it requires to introduce a new 10 – dim vector-like fermion  $F \sim (10, 1, 1)$  with mass  $M_F$  to trigger the bottom-top mass splitting. The colour triplet  $B$  component of  $F \sim (10, 1, 1)$  obtains the mass after Pati-Salam symmetry breaking:  $m_B \equiv y_F v_R / \sqrt{2} \sim 7000$  TeV, where we have used the same set of  $N_{F2} = 32$ ,  $N_{F3} = 108$ ,  $N_{F4} = 56$  above providing  $v_R \sim 10000$  TeV and  $y_F = 1$  at the Pati-Salam Symmetry breaking scale. By using Eq. (28), it requires  $M_F = \frac{\sqrt{2}m_B m_b}{m_t} = 239.2$  TeV to obtain the correct bottom quark mass. Since  $M_F$  is a free parameter in our theory, we do have the freedom to choose the desired value.

## 5 Conclusions

Models in which scalar degrees of freedom are fundamental a la Wilson [51, 52] require the presence of scale invariance at short distances [6, 53, 54]. A complete safe or free theory can therefore support elementary scalars as fundamental fields. Fundamentality and naturality are complementary concepts. Short distance scale invariance implies fundamentality while (near) long distance conformality and/or controllably broken symmetries help with naturality [6, 53]. A coherent search of safe extensions of the SM has only recently begun. In this work we have constructed a realistic safe extension of the SM in which we add vector-like fermions to the time-honored Pati-Salam framework. Recent progress in the large- $N$  safe dynamics of gauge-Yukawa theories has proven instrumental for the success of the project. In particular we have shown that the gauge, scalar quartic and Yukawa couplings achieve an interacting ultraviolet fixed point below the Planck scale. The minimal model is a relevant example of a Standard Model extension in which unification of *all* type of couplings occurs because of a dynamical principle, i.e. the presence of an ultraviolet fixed point. Most importantly, we are able to show that starting from specific UV fixed points, some of the RG flows can match both the SM Higgs mass and Yukawa couplings (top and bottom) which implies a truly UV completion of the Standard Model. It is also intriguing that, in this minimal model, the Pati-Salam symmetry breaking scale is close to  $10^4$  TeV to yield a physically acceptable Higgs mass. There are several aspects that deserve further investigation from a more in depth phenomenological study of the quark and lepton flavour sector to baryogenesis.

## 6 Acknowledgments

The work is partially supported by the Danish National Research Foundation under the grant D NRF:90 and the Natural Sciences and Engineering Research Council of Canada (NSERC). E. Molinaro thanks the Department of Physics and Astronomy of Aarhus University for the hospitality during the completion of this paper. Z.W. Wang thanks Robert Mann, Tom Steele, Heidi Rzehak, Chen Zhang and Jing Ren for very helpful suggestions.

## A One-Loop RG equations of the Pati-Salam model

### A.1 Gauge couplings

$$(4\pi)^2 \beta_{g_L} = -3g_L^3, \quad (45)$$

$$(4\pi)^2 \beta_{g_4} = -9g_4^3, \quad (46)$$

$$(4\pi)^2 \beta_{g_R} = -\frac{7}{3}g_R^3. \quad (47)$$

### A.2 Quartic coupling

$$(4\pi)^2 \beta_{\lambda_1} = \lambda_1 (32y_c^2 + 128\lambda_1 - 128\lambda_2 + 64\lambda_4 - 9g_L^2 - 9g_R^2 + 32y^2) + 512\lambda_2^2 + \frac{9}{32}(g_L^4 + g_R^4) + \frac{3}{16}g_L^2 g_R^2 + 32\lambda_{R\Phi 1} \lambda_{R\Phi 3} + 32\lambda_{R\Phi 1}^2 + 16\lambda_{R\Phi 3}^2 + 64\lambda_4^2 - 8y^4 - 8y_c^4, \quad (48)$$

$$(4\pi)^2 \beta_{\lambda_2} = \lambda_2 (32y^2 - 9g_L^2 - 9g_R^2 + 96\lambda_1 + 192\lambda_4 - 384\lambda_2 + 32y_c^2) - 4y_c^2 y^2 + 48\lambda_3^2 + 32\lambda_{R\Phi 2}^2, \quad (49)$$

$$(4\pi)^2 \beta_{\lambda_3} = \lambda_3 (32y_c^2 - 9g_L^2 - 9g_R^2 + 192\lambda_1 + 192\lambda_4 + 32y^2) - 8y^3 y_c - 8y y_c^3 + 64\lambda_{R\Phi 1} \lambda_{R\Phi 2} + 32\lambda_{R\Phi 2} \lambda_{R\Phi 3} \quad (50)$$

$$(4\pi)^2 \beta_{\lambda_4} = \lambda_4 (32y^2 - 9g_L^2 - 9g_R^2 + 96\lambda_1 + 128\lambda_2 + 64\lambda_4 + 32y_c^2) + \frac{3}{8}g_L^2 g_R^2 + 192\lambda_3^2 + 128\lambda_{R\Phi 2}^2 - 8\lambda_{R\Phi 3}^2 - 24y^2 y_c^2 + 4y_c^4 + 4y^4, \quad (51)$$

$$(4\pi)^2 \beta_{\lambda_{R1}} = \lambda_{R1} \left( 192\lambda_{R1} - 9g_R^2 - \frac{45}{2}g_4^2 + 192\lambda_{R2} + 20y_F^2 + 8y_\nu^2 \right) + 48\lambda_{R2}^2 + \frac{9}{32}g_R^4 + \frac{27}{128}g_4^4 + \frac{27}{32}g_R^2 g_4^2 + 16\lambda_{R\Phi 1}^2 + 16\lambda_{R\Phi 1} \lambda_{R\Phi 3} + 64\lambda_{R\Phi 2}^2 - \frac{1}{2}y_F^4 - 2y_\nu^4, \quad (52)$$

$$(4\pi)^2 \beta_{\lambda_{R2}} = \lambda_{R2} \left( -9g_R^2 - \frac{45}{2}g_4^2 + 20y_F^2 + 8y_\nu^2 + 96\lambda_{R1} \right) - \frac{9}{16}g_4^2 g_R^2 + \frac{9}{16}g_4^4 - 3y_F^4 + 8\lambda_{R\Phi 3}^2, \quad (53)$$

$$(4\pi)^2 \beta_{\lambda_{R\Phi 1}} = \lambda_{R\Phi 1} \left( 16y_c^2 + 16y^2 - \frac{9}{2}g_L^2 - \frac{45}{4}g_4^2 - 9g_R^2 + 80\lambda_1 - 64\lambda_2 + 32\lambda_4 + 144\lambda_{R1} + 96\lambda_{R2} + 10y_F^2 + 4y_\nu^2 \right) + 32\lambda_1 \lambda_{R\Phi 3} + 16\lambda_{R\Phi 1}^2 + 64\lambda_{R\Phi 2}^2 + 8\lambda_{R\Phi 3}^2 + \frac{9g_R^4}{16} + 64\lambda_{R1} \lambda_{R\Phi 3} - 64\lambda_2 \lambda_{R\Phi 3} + 32\lambda_4 \lambda_{R\Phi 3} + 16\lambda_{R2} \lambda_{R\Phi 3} - 4y_c^2 y_\nu^2 - 10y^2 y_F^2, \quad (54)$$

$$(4\pi)^2 \beta_{\lambda_{R\Phi 2}} = \lambda_{R\Phi 2} \left( 16y^2 + 16y_c^2 - \frac{9}{2}g_L^2 - 9g_R^2 - \frac{45}{4}g_4^2 + 16\lambda_1 + 64\lambda_2 + 64\lambda_4 + 144\lambda_{R1} + 96\lambda_{R2} + 10y_F^2 + 32\lambda_{R\Phi 1} + 16\lambda_{R\Phi 3} + 4y_\nu^2 \right) + 48\lambda_3 \lambda_{R\Phi 1} + 24\lambda_3 \lambda_{R\Phi 3} - 2y y_c y_\nu^2 - 5y y_c y_F^2, \quad (55)$$



$$\begin{aligned}
(4\pi)^2 \beta_{\lambda_{R\Phi 3}} = & \lambda_{R\Phi 3} \left( 16y^2 + 16y_c^2 - \frac{9}{2}g_L^2 - \frac{45}{4}g_4^2 + 16\lambda_1 + 64\lambda_2 - 32\lambda_4 + 16\lambda_{R1} \right. \\
& \left. + 64\lambda_{R2} + 10y_F^2 + 32\lambda_{R\Phi 1} + 4y_\nu^2 \right) + 16\lambda_{R\Phi 3}^2 - 10y_c^2 y_F^2 + 10y^2 y_F^2 \\
& + 4y_c^2 y_\nu^2 - 4y^2 y_\nu^2.
\end{aligned} \tag{56}$$

### A.3 Yukawa couplings

$$(4\pi)^2 \beta_y = -\frac{9y}{4}g_L^2 - \frac{9y}{4}g_R^2 - \frac{45y}{4}g_4^2 + 12y^3 + yy_\nu^2 + \frac{5}{2}yy_F^2, \tag{57}$$

$$(4\pi)^2 \beta_{y_c} = -\frac{9y_c}{4}g_L^2 - \frac{9y_c}{4}g_R^2 - \frac{45y_c}{4}g_4^2 + 12y_c^3 + y_c y_\nu^2 + \frac{5}{2}y_c y_F^2, \tag{58}$$

$$(4\pi)^2 \beta_{y_F} = -\frac{9y_F}{4}g_R^2 - \frac{153y_F}{8}g_4^2 + \frac{19}{2}y_F^3 - y_F y_\nu^2 + 2y^2 y_F, \tag{59}$$

$$(4\pi)^2 \beta_{y_\nu} = -\frac{9y_\nu}{4}g_R^2 - \frac{45y_\nu}{8}g_4^2 - \frac{5}{2}y_F^2 y_\nu + 11y_\nu^3 + 4y^2 y_\nu. \tag{60}$$

## References

- [1] D. F. Litim and F. Sannino, JHEP **1412**, 178 (2014) doi:10.1007/JHEP12(2014)178 [arXiv:1406.2337 [hep-th]].
- [2] D. F. Litim, M. Mojaza and F. Sannino, JHEP **1601**, 081 (2016) doi:10.1007/JHEP01(2016)081 [arXiv:1501.03061 [hep-th]].
- [3] F. Sannino, “ $\alpha_s$  at LHC: Challenging asymptotic freedom,” arXiv:1511.09022 [hep-ph]. Invited contribution for [4].
- [4] D. d’Enterria *et al.*, “Proceedings, High-Precision  $\alpha_s$  Measurements from LHC to FCC-ee : Geneva, Switzerland, October 2-13, 2015,” arXiv:1512.05194 [hep-ph].
- [5] S. Abel and F. Sannino, Phys. Rev. D **96**, no. 5, 056028 (2017) doi:10.1103/PhysRevD.96.056028 [arXiv:1704.00700 [hep-ph]].
- [6] G. M. Pelaggi, F. Sannino, A. Strumia and E. Vigiani, Front. in Phys. **5**, 49 (2017) doi:10.3389/fphy.2017.00049 [arXiv:1701.01453 [hep-ph]].
- [7] S. Abel and F. Sannino, Phys. Rev. D **96**, no. 5, 055021 (2017) doi:10.1103/PhysRevD.96.055021 [arXiv:1707.06638 [hep-ph]].
- [8] A. D. Bond, G. Hiller, K. Kowalska and D. F. Litim, JHEP **1708**, 004 (2017) doi:10.1007/JHEP08(2017)004 [arXiv:1702.01727 [hep-ph]].
- [9] K. Intriligator and F. Sannino, JHEP **1511**, 023 (2015) doi:10.1007/JHEP11(2015)023 [arXiv:1508.07411 [hep-th]].
- [10] S. P. Martin and J. D. Wells, Phys. Rev. D **64**, 036010 (2001) doi:10.1103/PhysRevD.64.036010 [hep-ph/0011382].
- [11] B. Bajc and F. Sannino, JHEP **1612**, 141 (2016) doi:10.1007/JHEP12(2016)141 [arXiv:1610.09681 [hep-th]].

- [12] A. D. Bond and D. F. Litim, Phys. Rev. Lett. **119**, no. 21, 211601 (2017) doi:10.1103/PhysRevLett.119.211601 [arXiv:1709.06953 [hep-th]].
- [13] B. Bajc, N. A. Dondi and F. Sannino, JHEP **1803**, 005 (2018) doi:10.1007/JHEP03(2018)005 [arXiv:1709.07436 [hep-th]].
- [14] K. S. Babu, B. Bajc and S. Saad, arXiv:1805.10631 [hep-ph].
- [15] A. Palanques-Mestre and P. Pascual, Commun. Math. Phys. **95**, 277 (1984). doi:10.1007/BF01212398
- [16] J. A. Gracey, Phys. Lett. B **373**, 178 (1996) doi:10.1016/0370-2693(96)00105-0 [hep-ph/9602214].
- [17] B. Holdom, Phys. Lett. B **694**, 74 (2011) doi:10.1016/j.physletb.2010.09.037 [arXiv:1006.2119 [hep-ph]].
- [18] C. Pica and F. Sannino, Phys. Rev. D **83**, 035013 (2011) doi:10.1103/PhysRevD.83.035013 [arXiv:1011.5917 [hep-ph]].
- [19] R. Shrock, Phys. Rev. D **89**, no. 4, 045019 (2014) doi:10.1103/PhysRevD.89.045019 [arXiv:1311.5268 [hep-th]].
- [20] F. Sannino and K. Tuominen, Phys. Rev. D **71**, 051901 (2005) doi:10.1103/PhysRevD.71.051901 [hep-ph/0405209].
- [21] D. D. Dietrich and F. Sannino, Phys. Rev. D **75**, 085018 (2007) doi:10.1103/PhysRevD.75.085018 [hep-ph/0611341].
- [22] F. Sannino, Acta Phys. Polon. B **40**, 3533 (2009) [arXiv:0911.0931 [hep-ph]].
- [23] C. Pica, PoS LATTICE **2016**, 015 (2016) doi:10.22323/1.256.0015 [arXiv:1701.07782 [hep-lat]].
- [24] O. Antipin and F. Sannino, Phys. Rev. D **97**, no. 11, 116007 (2018) doi:10.1103/PhysRevD.97.116007 [arXiv:1709.02354 [hep-ph]].
- [25] K. Kowalska and E. M. Sessolo, JHEP **1804**, 027 (2018) doi:10.1007/JHEP04(2018)027 [arXiv:1712.06859 [hep-ph]].
- [26] P. M. Ferreira, I. Jack and D. R. T. Jones, Phys. Lett. B **399**, 258 (1997) doi:10.1016/S0370-2693(97)00291-8 [hep-ph/9702304].
- [27] P. M. Ferreira, I. Jack, D. R. T. Jones and C. G. North, Nucl. Phys. B **504**, 108 (1997) doi:10.1016/S0550-3213(97)00448-3 [hep-ph/9705328].
- [28] G. M. Pelaggi, A. D. Plascencia, A. Salvio, F. Sannino, J. Smirnov and A. Strumia, Phys. Rev. D **97**, no. 9, 095013 (2018) doi:10.1103/PhysRevD.97.095013 [arXiv:1708.00437 [hep-ph]].
- [29] O. Antipin, N. A. Dondi, F. Sannino, A. E. Thomsen and Z. W. Wang, arXiv:1803.09770 [hep-ph].
- [30] T. Alanne and S. Blasi, arXiv:1806.06954 [hep-ph].

- [31] R. Mann, J. Meffe, F. Sannino, T. Steele, Z. W. Wang and C. Zhang, Phys. Rev. Lett. **119**, no. 26, 261802 (2017) doi:10.1103/PhysRevLett.119.261802 [arXiv:1707.02942 [hep-ph]].
- [32] J. McDowall and D. J. Miller, Phys. Rev. D **97**, no. 11, 115042 (2018) doi:10.1103/PhysRevD.97.115042 [arXiv:1802.02391 [hep-ph]].
- [33] S. Ipek, A. D. Plascencia and J. Turner, arXiv:1806.00460 [hep-ph].
- [34] A. Eichhorn, A. Held and P. V. Griend, arXiv:1802.08589 [hep-ph].
- [35] A. Eichhorn, A. Held and C. Wetterich, Phys. Lett. B **782**, 198 (2018) doi:10.1016/j.physletb.2018.05.016 [arXiv:1711.02949 [hep-th]].
- [36] M. Reichert, A. Eichhorn, H. Gies, J. M. Pawłowski, T. Plehn and M. M. Scherer, Phys. Rev. D **97**, no. 7, 075008 (2018) doi:10.1103/PhysRevD.97.075008 [arXiv:1711.00019 [hep-ph]].
- [37] A. Eichhorn, S. Lippoldt and V. Skrinjar, Phys. Rev. D **97**, no. 2, 026002 (2018) doi:10.1103/PhysRevD.97.026002 [arXiv:1710.03005 [hep-th]].
- [38] A. Eichhorn and F. Versteegen, JHEP **1801**, 030 (2018) doi:10.1007/JHEP01(2018)030 [arXiv:1709.07252 [hep-th]].
- [39] H. Georgi and S. L. Glashow, Phys. Rev. Lett. **32**, 438 (1974). doi:10.1103/PhysRevLett.32.438
- [40] J. C. Pati and A. Salam, Phys. Rev. D **10**, 275 (1974) Erratum: [Phys. Rev. D **11**, 703 (1975)]. doi:10.1103/PhysRevD.10.275, 10.1103/PhysRevD.11.703.2
- [41] P. Minkowski, Phys. Lett. **67B**, 421 (1977). doi:10.1016/0370-2693(77)90435-X
- [42] T. Yanagida, Conf. Proc. C **7902131**, 95 (1979).
- [43] M. Gell-Mann, P. Ramond and R. Slansky, Conf. Proc. C **790927**, 315 (1979) [arXiv:1306.4669 [hep-th]].
- [44] R. N. Mohapatra and G. Senjanovic, Phys. Rev. Lett. **44**, 912 (1980). doi:10.1103/PhysRevLett.44.912
- [45] R. R. Volkas, Phys. Rev. D **53**, 2681 (1996) doi:10.1103/PhysRevD.53.2681 [hep-ph/9507215].
- [46] C. Pica and F. Sannino, Phys. Rev. D **83**, 116001 (2011) doi:10.1103/PhysRevD.83.116001 [arXiv:1011.3832 [hep-ph]].
- [47] G. Valencia and S. Willenbrock, Phys. Rev. D **50**, 6843 (1994) doi:10.1103/PhysRevD.50.6843 [hep-ph/9409201].
- [48] D. Ambrose *et al.* [BNL Collaboration], Phys. Rev. Lett. **81**, 5734 (1998) doi:10.1103/PhysRevLett.81.5734 [hep-ex/9811038].
- [49] M. K. Parida, R. L. Awasthi and P. K. Sahu, JHEP **1501**, 045 (2015) doi:10.1007/JHEP01(2015)045 [arXiv:1401.1412 [hep-ph]].

- [50] M. Holthausen, M. Lindner and M. A. Schmidt, *Phys. Rev. D* **82**, 055002 (2010) doi:10.1103/PhysRevD.82.055002 [arXiv:0911.0710 [hep-ph]].
- [51] K. G. Wilson, *Phys. Rev. B* **4**, 3174 (1971). doi:10.1103/PhysRevB.4.3174
- [52] K. G. Wilson, *Phys. Rev. B* **4**, 3184 (1971). doi:10.1103/PhysRevB.4.3184
- [53] O. Antipin, M. Mojaza and F. Sannino, *Phys. Rev. D* **89**, no. 8, 085015 (2014) doi:10.1103/PhysRevD.89.085015 [arXiv:1310.0957 [hep-ph]].
- [54] M. Shaposhnikov and A. Shkerin, arXiv:1804.06376 [hep-th].
- [55] G. C. Branco, P. M. Ferreira, L. Lavoura, M. N. Rebelo, M. Sher and J. P. Silva, *Phys. Rept.* **516** (2012) 1 [arXiv:1106.0034 [hep-ph]].
- [56] W. F. Chang, T. Modak and J. N. Ng, *Phys. Rev. D* **97** (2018) no.5, 055020 [arXiv:1711.05722 [hep-ph]].
- [57] G. Dupuis, *JHEP* **1607** (2016) 008 [arXiv:1604.04552 [hep-ph]].